Surface-Enhanced and Normal Stokes and Anti-Stokes Raman Spectroscopy of Single-Walled Carbon Nanotubes

K. Kneipp,[1,5] H. Kneipp,[1,5] P. Corio,[2] S. D. M. Brown,[2] K. Shafer,[1] J. Motz,[1] L. T. Perelman,[1]
E. B. Hanlon,[1] A. Marucci,[2] G. Dresselhaus,[3] and M. S. Dresselhaus[2,4]

[1]*George R. Harrison Spectroscopy Laboratory, Massachusetts Institute of Technology, Cambridge, Massachusetts 02139*
[2]*Department of Physics, Massachusetts Institute of Technology, Cambridge, Massachusetts 02139*
[3]*Francis Bitter Magnet Laboratory, Massachusetts Institute of Technology, Cambridge, Massachusetts 02139*
[4]*Department of Electrical Engineering and Computer Science, Massachusetts Institute of Technology,*
Cambridge, Massachusetts 02139
[5]*Department of Physics, Technical University of Berlin, Berlin, Germany*
(Received 26 July 1999)

Surface enhancement factors of at least 10^{12} for the Raman scattering of single-walled carbon nanotubes in contact with fractal silver colloidal clusters result in measuring very narrow Raman bands corresponding to the homogeneous linewidth of the tangential C–C stretching mode in semiconducting nanotubes. Normal and surface-enhanced Stokes and anti-Stokes Raman spectra are discussed in the framework of selective resonant Raman contributions of semiconducting or metallic nanotubes to the Stokes or anti-Stokes spectra, respectively, of the population of vibrational levels due to the extremely strong surface-enhanced Raman process, and of phonon-phonon interactions.

Single-walled carbon nanotubes (SWNTs) are macromolecules with remarkable properties (mechanical, electronic, thermal stability, thermal conductivity, etc.) [1,2]. Nanotubes are normally found in bundles and/or ropes [3], containing both semiconducting and metallic SWNTs, which have a significantly different electronic density of states (DOS) and different phonon spectra [1,2]. Not only does Raman scattering (RS) probe the phonon spectra of carbon nanotubes but also, in resonance Raman scattering (RRS), the excitation profile provides information about the 1D electronic DOS of the nanotubes [4,5].

The Raman signal can be enhanced by many orders of magnitude for molecules attached to metallic nanostructures. This effect, known as surface-enhanced Raman scattering (SERS) [6,7], which allows Raman spectroscopy to probe single molecules [8–10], also offers exciting opportunities for studying nanotubes. Additional information is provided by exploiting Raman scattering at the high-energy anti-Stokes side of the excitation laser. According to simple Raman theory and demonstrated by many experiments, one expects the anti-Stokes spectrum to display the same Raman shifts as the Stokes spectrum. In this paper, we describe differences between the Stokes and anti-Stokes spectra using the same laser excitation energy. These differences arise from the fact that Stokes scattering can selectively probe metallic nanotubes while anti-Stokes scattering probes semiconducting nanotubes (or vice versa) due to the different RRS conditions for semiconducting and metallic nanotubes. The strength of the anti-Stokes Raman signal depends on the population of the first excited vibrational states. Normally, this population is determined by the Boltzmann distribution, and, in this way, the anti-Stokes signal strength provides information on the sample temperature. But the strength of the anti-Stokes

signal can also monitor other processes that populate excited vibrational states in excess of thermal equilibrium [8], as we discuss below in more detail for SWNTs.

In this study, "normal" and surface-enhanced Stokes and anti-Stokes Raman scattering are used to extract information on single SWNTs. Recently, surface-enhanced Fourier transform Raman spectroscopy was applied to study SWNTs deposited on rough gold and silver surfaces prepared by evaporation [11]. In our SERS experiments, we attach the SWNTs to fractal silver colloidal clusters. A very inhomogeneous field distribution over the silver clusters, including extremely large electromagnetic fields in the so-called "hot areas" [12–14], provide the key effect for extremely large SERS enhancement factors (up to 10^{14}) as are observed on such fractal structures [8,9].

A silver colloidal cluster solution was prepared as previously described [8,9] and SWNTs were added in low concentrations. For some samples, ultrasound was applied in order to break up the bundles. About 50 μl of the sample solution were evaporated on a microscopic cover slide. Figure 1(a) shows a section of a nanotube bundle, with a colloidal silver cluster touching the end of the bundle. No Raman signal was collected from such a bundle if it was not in contact with the colloidal silver (collection point No. 1). Figure 1 shows that SERS spectra appear, as the laser comes closer to the cluster (collection point No. 2), and the SERS spectrum grows much more intense when the SWNTs touch the Ag cluster (collection point No. 3).

The lower part of Fig. 2 shows surface-enhanced and normal Raman scattering (NRS) Stokes (S) and anti-Stokes (AS) spectra of SWNTs in the range of the tangential C–C stretching modes, while in the upper part of Fig. 2 the Stokes and anti-Stokes SERS signal heights P_S and
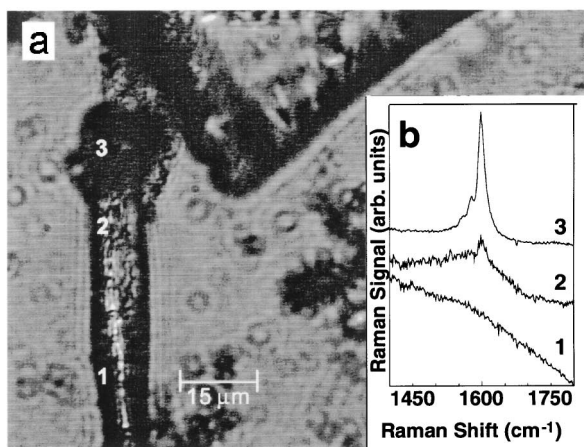
0031-9007/00/84(15)/3470(4)$15.00

FIG. 1. Microscope view of (a) a section of a nanotube bundle touching a colloidal Ag cluster, and (b) SERS spectra collected along various points (1, 2, 3) on the bundle, using 830 nm cw Ti:sapphire laser excitation with a 1 μm spot size. The black spots in (a) are colloidal silver particles of different sizes that are aggregated by addition of NaCl [8].

P_{AS} are plotted as a function of the incident laser intensity I_L. In both the NRS and SERS cases, different spectral features appear at the low- and high-energy sides of the 830 nm excitation laser. The Stokes spectrum is characteristic of that for semiconducting nanotubes, whereas the anti-Stokes spectrum is characteristic of that from metallic nanotubes. The anti-Stokes/Stokes asymmetry is related to the RRS process in the SWNT bundles, which contain both semiconducting and metallic nanotubes. Very briefly, in RRS, incident and/or scattered photons are in resonance with an electronic transition. Therefore, the scattered photons for Stokes and anti-Stokes processes will be in resonance with nanotubes having different (n, m) integers. At 830 nm excitation, the Stokes scattering (which is shifted to $\sim$955 nm) appears from resonant semiconducting nanotubes (strongest phonon line near 1592 cm^{-1}), whereas the anti-Stokes Raman scattering (which is shifted to $\sim$735 nm) benefits from resonance enhancement of metallic nanotubes, and therefore features near 1580 and 1540 cm^{-1} associated with metallic nanotubes appear at the anti-Stokes side. To further illustrate the asymmetry between the Stokes and anti-Stokes spectra, Fig. 3 shows the situation for shorter excitation wavelengths. At 647 nm excitation, Stokes scattering benefits more from resonance with metallic nanotubes, and therefore metallic nanotube contributions dominate the Stokes spectrum. At 647 nm excitation, the anti-Stokes wavelength is nearly out of the range for metallic electronic transitions, which is reflected in a large decrease in the metallic contribution to the anti-Stokes spectrum. The effect of selective contributions of metallic and semiconducting nanotubes at the low- and high-energy sides of the excitation laser will be quantitatively discussed elsewhere [15]. To complete our qualitative discussion here, Fig. 3 shows that both the Stokes and anti-Stokes wavelengths are out of the resonance range for metallic nanotubes for
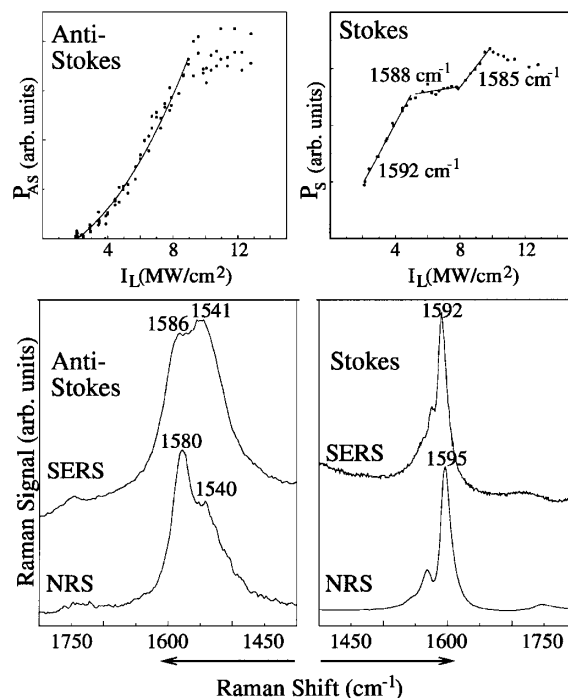

FIG. 2. Lower plots show SERS and NRS anti-Stokes and Stokes spectra of SWNTs measured with 830 nm (1.49 eV) excitation. On the top are plots of surface-enhanced anti-Stokes (left) and Stokes (right) signal heights P_{AS} and P_S vs excitation laser intensity I_L. The lines display linear (right) and quadratic (left) fits to the experimental data [see Eq. (1)]. The center of the Stokes SERS band shifts from 1592 cm^{-1} to 1588 cm^{-1} to 1585 cm^{-1} with increasing I_L, as P_S changes from one slope to another. At $I_L \sim 10$ MW/cm^2, irreversible destruction of the nanotube starts.

514 nm excitation, so that both Stokes and anti-Stokes signals come from semiconducting nanotubes, which are about twice as numerous as metallic nanotubes in the nanotube bundles [1,2].

A comparison of normal and surface-enhanced spectra in Figs. 2 and 3 regarding the general spectral features and the relative signal strengths shows that the SERS spectra are basically the same as the NRS spectra, implying that all corresponding phonon modes are enhanced by similar amounts. The small differences between the NRS and SERS phonon frequencies and enhancement levels are discussed in a separate paper, where SERS data from silver and gold films are also compared [16].

In NRS experiments on nanotubes, heating of the sample occurs, which is reflected in the relatively strong anti-Stokes signals. In SERS, the heating effect is very small due to the efficient heat transfer to the silver. This can be concluded from Fig. 2 (top right) by the following argument. Between 2 and $\sim$5 MW/cm^2, the Stokes SERS signal increases linearly with I_L and no frequency shift is observed for the center of the Stokes band of the semiconducting nanotubes (1592 cm^{-1}), indicating very little increase in temperature, too little to result in a measurable frequency shift, as is observed, for example, in the dependence of the normal Raman spectra of SWNTs on
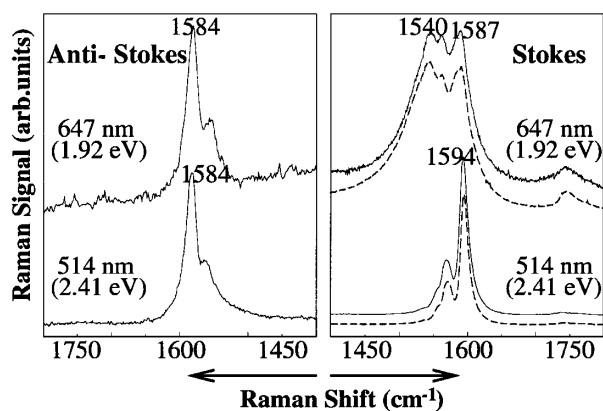
FIG. 3. NRS Stokes and anti-Stokes spectra (solid curve) of SWNTs in the tangential C−C stretching mode range and SERS Stokes spectra (dashed curve), all measured at 647 and 514 nm excitation (see text). For laser excitation in the visible range, the anti-Stokes SERS spectra near 1600 cm^{-1} were too weak to be detected.

I_L due to heating [17]. The frequency shift of the center of the Stokes band in Fig. 2 (top right) can be explained by different contributions of the E_{2g}, A_{1g}, and E_{1g} modes that constitutes this tangential band [2]. Through phonon-phonon coupling at the very large laser intensities I_L, these phonons can couple and exchange energy. Further studies are underway to explain this effect, as well as the different slopes of the signal height of the center of the band vs I_L.

The anti-Stokes SERS signal in Fig. 2 originates from metallic nanotubes and appears as a broad band from 1540–1580 cm^{-1}. This signal is nonlinearly dependent on laser intensity between 2 and ∼10 MW/cm^2 (see Fig. 2, top left). This nonlinearity can be due to two effects: increasing temperature T with increasing laser intensity, and/or vibrational pumping. In the second mechanism, a very large Raman effect populates vibrational levels in excess of the normal Boltzmann population [8]. Vibrational pumping can be observed only at extremely large effective Raman cross sections and is an indication of a very high SERS enhancement level [8].

A simple theoretical estimate for the Stokes and anti-Stokes power levels P_S and P_{AS} can be derived from a rate equation model describing the population/depopulation of the first excited vibrational level by SERS Stokes and anti-Stokes transitions [8]. In the steady state, assuming that we are far from saturation of the vibrational transition, P_{AS} and P_S can be expressed as

$$P_{AS} \simeq \left[\exp\left(\frac{-h\nu}{kT(n_L)}\right) + \tau_1 n_L \sigma_M^{SERS} \right] N_M n_L \sigma_M^{SERRS},$$

$$P_S \simeq N_{SC} n_L \sigma_{SC}^{SERRS},$$ (1)

where N_M and N_{SC} are the numbers of metallic (M) and semiconducting (SC) nanotubes in the vibrational ground state that interact with the laser beam, σ_M^{SERS} and σ_{SC}^{SERS} are the effective nonresonant SERS cross sections, while

the superscript SERRS refers to the resonant process, ν is the phonon frequency, τ_1 is the phonon lifetime, T is the sample temperature, and n_L is the photon flux density of the laser corresponding to I_L in Fig. 2 (top). It should be noted that the effective SERS cross sections describe the total enhancement including "electromagnetic field" enhancement and "chemical" enhancement (see also discussion below). The anti-Stokes signal P_{AS} shows a quadratic dependence on n_L, whereas the Stokes signal P_S remains linearly dependent on n_L. Figure 2 shows linear fits of the experimental Stokes P_S to three ranges of I_L, each range having a different slope (see above).

Fits to the anti-Stokes SERS signal P_{AS} as a function of I_L were carried out, including both heating and vibrational pumping effects. Fits using the "temperature model" [first term in Eq. (1)] and also to the "pumping model" [second term in Eq. (1)] have comparable root mean square errors up to $I_L \sim 10$ MW/cm^2. However, the heating model requires temperatures of ∼1200 K for the metallic nanotubes at 5 MW/cm^2 laser intensity. Such a high temperature seems unlikely, because the semiconducting nanotubes, which are even in better resonance with the 830 nm laser photons than the metallic tubes, are almost unheated up to 5 MW/cm^2 laser intensity, since, as discussed above, essentially no Raman shift in the Stokes P_S signal is observed. Another argument against strong laser heating in SERS experiments comes from the absence of an anti-Stokes SERS signal at shorter excitation wavelengths (647 and 514 nm, see Fig. 3), where heating of metallic nanotubes also occurs, but, according to theory [13,14], the field enhancement effect is not as strong. The missing anti-Stokes signals for SERS and the strong anti-Stokes signals in NRS for visible excitation are therefore indications that increased temperature cannot be the key mechanism for strong anti-Stokes SERS signals at 830 nm excitation. Thus, we infer that vibrational pumping gives the dominant contribution to the observed nonlinear dependence of the anti-Stokes signal. From the fitting parameters, we conclude that the product of the cross section and the lifetime for the nonresonant Stokes Raman process for metallic nanotubes is on the order of 5×10^{-28} cm^2 s. This process determines the population of the phonon levels of the metallic SWNTs that we probe in the resonant anti-Stokes process. Assuming a vibrational lifetime on the order of 10 ps for the phonons of the metallic nanotubes (in good agreement with the measured linewidth in Fig. 4), an effective Raman cross section on the order of about 10^{-16} cm^2 must be operative. Starting from intrinsic nonresonant Raman cross sections between 10^{-30}–10^{-28} cm^2 for the metallic nanotubes, as are measured for many compounds [18], a cross section of 10^{-16} cm^2 could be reached by SERS enhancement factors on the order of 10^{12}–10^{14}. Electromagnetic field enhancement in hot areas of fractal structures [13,14] can provide enhancement factors of 10^{10}–10^{12}. There are likely additional enhancement effects based on the electronic interaction of the nanotubes with the metal surface which are
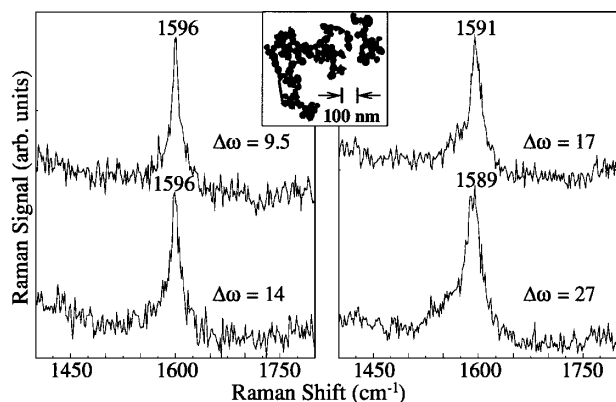
FIG. 4. Typical fractal colloidal silver clusters (see inset) and selected SERS spectra of the tangential band, with a linewidth $\Delta\omega$ (in cm^{-1}) as small as 9.5 cm^{-1}, collected from such a cluster area at 830 nm laser excitation with 1 μm spot size.

expected to be different for metallic and semiconducting nanotubes. These chemical enhancement effects can contribute an additional factor of 10 to 100 [6], thus yielding the enhancement factors of 10^{12}–10^{14}, which are also consistent with experimental values in single molecule SERS studies on colloidal metal structures [8,9]. Such enhancement factors provide hope for observing Raman spectra from very small numbers of nanotubes, perhaps down to a single nanotube.

Figure 4 shows a typical collection of colloidal silver clusters and selected SERS Stokes spectra, measured in 1 s collection times, while scanning over silver cluster areas containing only a very small number of nanotubes. The linewidths of the Raman signals are smaller than those measured in NRS. The narrowest measured linewidth in Fig. 4 at 1596 cm^{-1} was 9.5 cm^{-1}, which is very close to the homogeneous linewidth of the tangential C–C stretching mode in semiconducting SWNTs deduced from a natural FWHM linewidth of 4 cm^{-1} and theoretical estimates for the frequencies of the E_{2g}, A_{1g}, and E_{1g} modes [2], which contribute to this band and are estimated to differ from one another by only 6 cm^{-1}. This indicates that tubes of a unique diameter or perhaps even a single nanotube might contribute to the Raman signal. The strong enhancement and confinement of the electromagnetic field on a silver cluster, within domains that can be as small as 20 nm [19], may provide an additional high lateral resolution tool for selectively probing the small numbers of nanotubes that are adjacent to the interface just in such a domain. Even stronger SERS enhancement is expected at low Raman frequency shifts [13,14]. Thus, it may be possible for SERS to reveal the radial breathing mode band for individual SWNTs, free from the inhomogeneous broadening effects observed for this mode in normal resonant Raman spectra.

One of us (K. K.) would like to thank Professor M. S. Feld and Dr. R. R. Dasari for their kind hospitality and support of this research, as well as for many stimulating

[1] M. S. Dresselhaus, G. Dresselhaus, and P. C. Eklund, *Science of Fullerenes and Carbon Nanotubes* (Academic Press, New York, 1996).

[2] R. Saito, G. Dresselhaus, and M. S. Dresselhaus, *Physical Properties of Carbon Nanotubes* (Imperial College Press, London, 1998).

[3] A. Thess, R. Lee, P. Nikolaev, H. Dai, P. Petit, J. Robert, C. Xu, Y. H. Lee, S. G. Kim, A. G. Rinzler, D. T. Colbert, G. E. Scuseria, D. Tománek, J. E. Fischer, and R. E. Smalley, Science **273**, 483 (1996).

[4] A. M. Rao, E. Richter, S. Bandow, B. Chase, P. C. Eklund, K. W. Williams, M. Menon, K. R. Subbaswamy, A. Thess, R. E. Smalley, G. Dresselhaus, and M. S. Dresselhaus, Science **275**, 187 (1997).

[5] M. A. Pimenta, A. Marucci, S. Empedocles, M. Bawendi, E. B. Hanlon, A. M. Rao, P. C. Eklund, R. E. Smalley, G. Dresselhaus, and M. S. Dresselhaus, Phys. Rev. B **58**, R16 016 (1998).

[6] A. Otto, in *In Light Scattering in Solids IV. Electronic Scattering, Spin Effects, SERS and Morphic Effects,* edited by M. Cardona and G. Guntherodt (Springer-Verlag, Berlin, 1984).

[7] M. Moskovits, Rev. Mod. Phys. **57**, 783 (1985).

[8] K. Kneipp, Y. Wang, H. Kneipp, I. Itzkan, R. R. Dasari, and M. S. Feld, Phys. Rev. Lett. **76**, 2444 (1996).

[9] K. Kneipp, Y. Wang, H. Kneipp, L. T. Perelman, I. Itzkan, R. R. Dasari, and M. S. Feld, Phys. Rev. Lett. **78**, 1667 (1997).

[10] S. Nie and S. R. Emory, Science **275**, 1102 (1997).

[11] S. Lefrant, I. Baltog, M. Lamy de la Chapelle, M. Baibarac, G. Louarn, C. Journet, and P. Bernier, Synth. Met. **100**, 13 (1999).

[12] V. M. Shalaev and M. I. Stockman, Sov. Phys. JETP **65**, 287 (1987).

[13] M. I. Stockman, V. M. Shalaev, M. Moskovits, R. Botet, and T. F. George, Phys. Rev. B **46**, 2821 (1992).

[14] V. A. Markel, V. M. Shalaev, P. Zhang, W. Huynh, L. Tay, T. L. Haslett, and M. Moskovits, Phys. Rev. B **59**, 10 903 (1999).

[15] S. D. M. Brown, P. Corio, A. Marucci, M. S. Dresselhaus, M. A. Pimenta, and K. Kneipp, Phys. Rev. B **61**, R5137 (2000).

[16] P. Corio, S. D. M. Brown, A. Marucci, M. A. Pimenta, M. S. Dresselhaus, and K. Kneipp, Phys. Rev. B (to be published).

[17] F. Huang, K. T. Yue, P. Tan, S. L. Zhang, Z. Shi, X. Zhou, and Z. Gu, J. Appl. Phys. **84**, 4022 (1998).

[18] A. Weber, in *Raman Spectroscopy in Gases and Liquids* (Springer, New York, 1979).

[19] V. P. Safonov, V. M. Shalaev, V. A. Markel, Yu. E. Danilova, N. N. Lepeshkin, W. Kim, S. G. Rautian, and R. L. Armstrong, Phys. Rev. Lett. **80**, 1102 (1998).